Structure of weak shocks in fluids having embedded regions of negative nonlinearity

M. S. Cramer

Citation: Physics of Fluids (1958-1988) **30**, 3034 (1987); doi: 10.1063/1.866082
View online: http://dx.doi.org/10.1063/1.866082
View Table of Contents: http://scitation.aip.org/content/aip/journal/pof1/30/10?ver=pdfcov
Published by the AIP Publishing

Structure of weak shocks in fluids having embedded regions of negative nonlinearity

M. S. Cramer
Department of Engineering Science and Mechanics, Virginia Polytechnic Institute and State University, Blacksburg, Virginia 24061

(Received 26 March 1987; accepted 19 June 1987)

The dissipative structure of weak shock waves in fluids in which the fundamental derivative is negative for a finite range of pressures and temperatures has been examined. Conditions under which the shock thickness increases with strength rather than decreases are delineated. Nonclassical features of the entropy distribution and variation of local Mach number are also described.

I. INTRODUCTION

The nature of shock waves in single-phase fluids is determined by the quantity

$$\bar{\Gamma}(\bar{\rho},\bar{s}) = \frac{\bar{a}}{\bar{\rho}} + \frac{\partial \bar{a}}{\partial \bar{\rho}}\bigg|_{\bar{s}}, \tag{1}$$

where $\bar{a} = \bar{a}(\bar{\rho},\bar{s})$ is the thermodynamic sound speed, $\bar{\rho}$ is the density, and $\bar{s}$ is the entropy; in all that follows, the overbar denotes dimensional quantities. This parameter is uniquely determined by the thermodynamic state of the fluid and is frequently referred to as the fundamental derivative of gas dynamics. When $\bar{\Gamma} > 0$ (positive nonlinearity) the only shocks possible are compression shocks; this case is typical of many gases and liquids at normal temperatures and pressures. When $\bar{\Gamma} < 0$ (negative nonlinearity) compression shocks violate the entropy inequality and the only shocks possible are expansion shocks. A number of authors[1–4] have shown that (1) may become negative in fluids in which the specific heat is sufficiently large; the pressures and temperatures required are on the order of those at the thermodynamic critical point. In particular, Lambrakis and Thompson[3] and Thompson and Lambrakis[4] have given a number of specific fluids of practical interest in which a region of negative $\bar{\Gamma}$ is likely to occur. Contours of constant $\bar{\rho}\bar{\Gamma}/\bar{a}$ are plotted in Fig. 1 for the case of a van der Waals gas with a large, but constant, specific heat. The variation of $\bar{\rho}\bar{\Gamma}/\bar{a}$ at constant energy is depicted in Fig. 2 for the same gas as in Fig. 1. The rate of change of $\bar{\Gamma}$ is also of interest in the present study and the variation of the nondimensional quantity,

$$\Lambda(\bar{\rho},\bar{s}) = \frac{\bar{\rho}^2}{\bar{a}}\frac{\partial \bar{\Gamma}}{\partial \bar{\rho}}\bigg|_{\bar{s}}, \tag{2}$$

is plotted in Fig. 3.

Equations of state are frequently given in terms of the specific volume and absolute temperature. Convenient expressions for (1) in terms of the derivatives of these quantities have been given by previous authors.[1,3,4] The corresponding expressions for (2) for arbitrary gases are given in the Appendix of the present study.

If the variations in the pressure and temperature are such that the fundamental derivative (1) changes sign from point to point in a given flow field, the dynamics of the fluid are seen to be qualitatively different from that observed in ideal gases or, more generally, when $\bar{\Gamma}$ is strictly positive or strictly negative.[4–8] Of direct interest to the present study is the weak shock theory developed by Cramer and Kluwick.[5] The disturbance amplitudes were taken to be small and the undisturbed state of the fluid was taken to be close to the $\bar{\Gamma} = 0$ locus. Thus even small disturbances may result in a change in the sign of the local value of the fundamental derivative. Although the variation of density and temperature in many shocks is qualitatively the same as that for weak shocks in perfect gases, the structure of sonic shocks was found to be fundamentally different. Sonic shocks are shock waves which have a speed identical to either the upstream or downstream value of the convected sound speed. It was shown that the density approaches the inviscid conditions algebraically rather than exponentially at the sonic side of the shock. A similar result has been reported in the context of shear waves in viscoelastic solids.[9] This relatively slow approach suggests that sonic and near-sonic shocks may be thicker than shocks of the same strength in perfect gases.

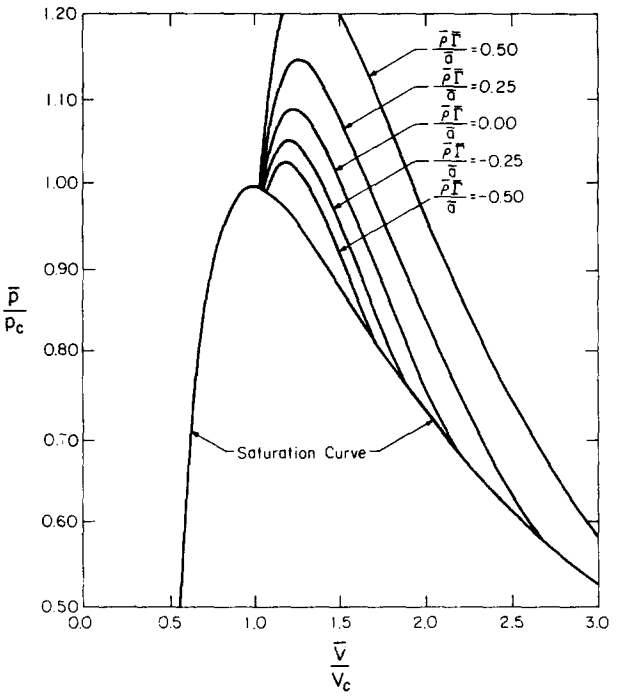

FIG. 1. Contours of constant $\bar{\rho}\bar{\Gamma}/\bar{a}$. Gas model is that of van der Waals with a constant specific heat equal to $\bar{c}_v = 50R$, where R is the gas constant. The subscript c denotes properties at the thermodynamic critical point.

 0031-9171/87/103034-11$01.90

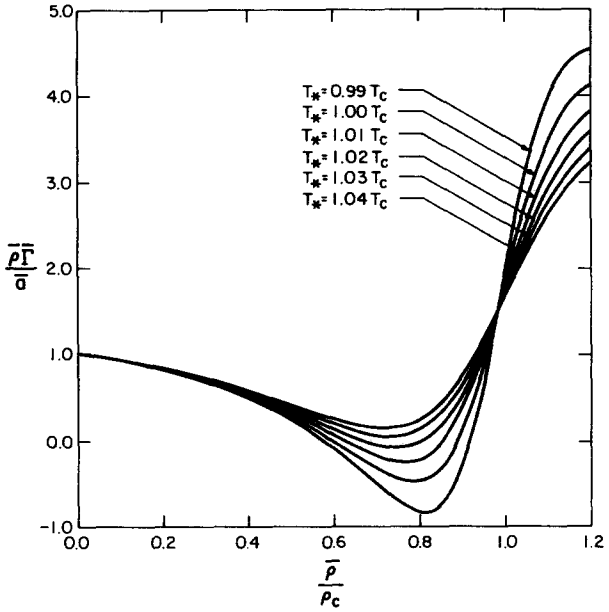

FIG. 2. Variation of $\bar{\rho}\bar{\Gamma}/\bar{a}$ on isentropes. Gas model is the same as in Fig. 1. The quantity T_* is a reference temperature such that each isentrope goes through the point $\bar{\rho} = 0.5\rho_c$, $\bar{T} = T_*$.

The present study shows that these effects lead to a local minimum in the thickness of the shocks. This contrasts with the classical results, which predict that the thickness decreases monotonically with increasing shock strength.

In both experimental and numerical studies of these fluids, it is necessary to distinguish between a thick shock and one which has disintegrated by the inviscid mechanisms described in previous studies.[5,6,8] The estimates given here are expected to be useful when this distinction is necessary. Experimental studies which employ shock waves to determine transport or dissipation coefficients of the fluids treated here may be misinterpreted if the local minimum in the shock thickness is not taken into account. From the results described in Sec. III, it should be clear that an anomalous increase in the dissipation coefficients would be incorrectly predicted if the thickness is assumed to decrease with shock strength.

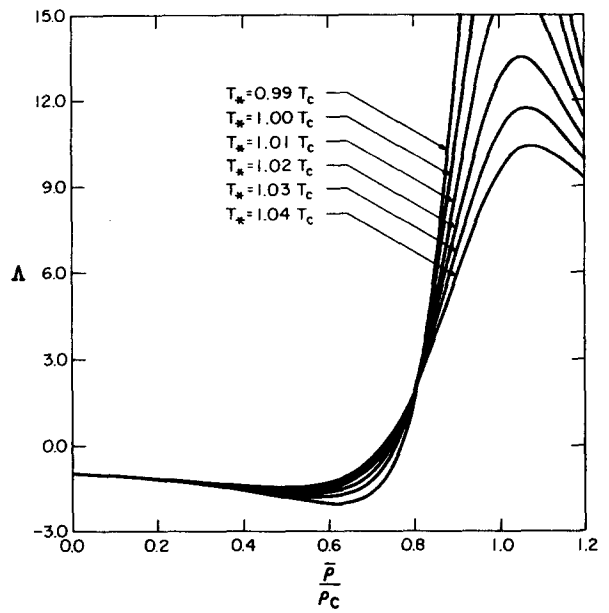

FIG. 3. Variation of Λ on isentropes. Gas model is the same as in Fig. 1. The quantity T_* is a reference temperature such that each isentrope goes through the point $\bar{\rho} = 0.5\rho_c$, $\bar{T} = T_*$.

In inviscid theories the values of entropy and Mach number before and after the shock are used to eliminate inadmissible discontinuities. Sections IV and V provide a discussion of the transition of these crucial properties between the upstream and downstream states. In both cases, the qualitative behavior can differ from that known to occur in perfect gases. Explicit formulas for the entropy distribution are given in Sec. IV for weak shocks. Expansion shocks are shown to be characterized by an initial decrease in entropy which is overcome in admissible shocks to generate a net increase in entropy across the shock. In Sec. V it is shown that the Mach number variation is nonclassical when the fundamental derivative (1) changes sign across the shock. The Mach number is seen to attain either a local maximum or minimum at the point at which $\bar{\Gamma} = 0$. This lack of monotonic behavior is also expected to be of interest outside of the immediate context. As an example, the present results suggest a mechanism for the transition of the Mach number in double sonic shocks. Such shocks have a finite strength, but both upstream and downstream Mach numbers are unity.[4,8] If the present results are extrapolated it would appear that the Mach number will oscillate about the sonic condition. A maximum and minimum should be observed corresponding to the two changes in the sign of $\bar{\Gamma}$. However, it must be recognized that double-sonic shocks are normally of finite amplitude and a more extensive study of the entropy variation will be needed before such an extrapolation of our weak shock results may be regarded as appropriate.

The result for the shock thickness, Mach number, and entropy variation will strongly depend on the solutions for the density variations derived in Ref. 5. Section II will review these results and introduce notation which will be convenient in the subsequent sections. To clarify the picture of the range of shocks possible in these fluids the results of Cramer and Kluwick[5] will be discussed in the context of the shock adiabat. It is expected that this discussion will assist in the physical interpretation of the result of Secs. III–V, as well as those of Refs. 5 and 6.

II. RESULTS FOR THE DENSITY VARIATION

The usual model for the dissipative structure of a shock wave is that the flow is one-dimensional and steady. Flow variables such as density, temperature, and particle velocity are taken to approach constants far upstream and downstream of the shock. The case examined by Cramer and Kluwick[5] takes the shock to be weak and the unperturbed state to be close to the $\bar{\Gamma} = 0$ locus, i.e.,

$$\Gamma = O[(\bar{\rho} - \rho_0)/\rho_0] = o(1), \quad \Lambda = O(1). \tag{3}$$

The quantity

$$\Gamma \equiv \rho_0 \bar{\Gamma}(\rho_0, s_0)/a_0 \tag{4}$$

is recognized as a nondimensional version of the fundamental derivative (1). The subscript 0 denotes dimensional quantities evaluated at the unperturbed state. The solution for the density perturbation was found to be

$$\frac{\bar{\rho}-\rho_0}{\rho_0}=\sigma\frac{\rho_a-\rho_b}{2\rho_0}G+\frac{1}{2}\left(\frac{\rho_a-\rho_0}{\rho_0}+\frac{\rho_b-\rho_0}{\rho_0}\right), \tag{5}$$

where the subscripts a and b denote dimensional quantities evaluated at the state immediately after (downstream of) the shock and the state immediately before (upstream of) the shock, respectively. As in Refs. 5 and 6 the cases where $\Lambda>0$ and $\Lambda<0$ will be treated with the same set of formulas. In all that follows Λ will be taken to be the value of (2) evaluated at the perturbed state ρ_0, s_0. To accomplish this in the present study, the symbol σ has been introduced in (5) to denote the sign of Λ, i.e., $\sigma\equiv\Lambda/|\Lambda|$. In the original study by Cramer and Kluwick,[5] σ was not introduced and it was necessary to interchange directions of propagation and the subscripts a and b in formulas analogous to (5) when Λ was negative. To illustrate this convention we note that

$$(\bar{\rho}-\rho_0)/\rho_0=(1-\sigma)[(\rho_a-\rho_0)/2\rho_0]+(1+\sigma)[(\rho_b-\rho_0)/2\rho_0]$$

in the limit $G\to-1$. Thus, when $\Lambda>0$, i.e., $\sigma=1$, this limit corresponds to the upstream conditions $\bar{\rho}=\rho_b$. When $\Lambda<0$, i.e., $\sigma=-1$, $\rho\to\rho_a$, which corresponds to the downstream conditions. Analogous remarks hold for the limit $G\to1$. The function $G(\hat{\xi};B)$ is related to the scaled position $\hat{\xi}$ by

$$\hat{\xi}=\frac{1}{B^2-1}\left[2\ln\left(\frac{G+B}{B}\right)+B\ln\left(\frac{1-G}{1+G}\right)-\ln(1-G^2)\right] \tag{6}$$

for $B>1$ and

$$\hat{\xi}=\frac{1}{2}\ln\left(\frac{1-G}{1+G}\right)-\frac{G}{1+G} \tag{7}$$

for $B=1$. The parameter B is identical to that of Ref. 5 and is given by

$$B\equiv\sigma\frac{6\Gamma}{\Lambda}\left[1+\frac{\Lambda}{2\Gamma}\left(\frac{\rho_a-\rho_0}{\rho_0}+\frac{\rho_b-\rho_0}{\rho_0}\right)\right]\frac{\rho_0}{\rho_a-\rho_b}. \tag{8}$$

For later use we note that the scaled position $\hat{\xi}$ is related to the actual position $\bar{x}$, as measured in a frame moving with the shock, by

$$\bar{x}=\sigma L_d(\Gamma^2/\Lambda^2)[\rho_0/(\rho_a-\rho_b)]^2\hat{\xi}, \tag{9}$$

where L_d is a nonlinear diffusion length defined by

$$L_d=\frac{|\Lambda|12\mu_0}{\Gamma^2 a_0\rho_0}\left(\frac{\lambda_0}{\mu_0}+2+\frac{\gamma_0-1}{\mathrm{Pr}}\right). \tag{10}$$

The quantities μ_0, λ_0, γ_0, and Pr are the shear viscosity, second viscosity, ratio of specific heats, and Prandtl number evaluated at the unperturbed state. The fact that σ appears in (9) implies that the results for $\Lambda>0$ and $\Lambda<0$ are related by a reflection of the $\bar{x}$ axis; this is consistent with the relationships given in both Refs. 5 and 6.

The function G is plotted in Fig. 4 for various values of $B\geqslant1$. The condition $B=1$ corresponds to a sonic shock; the thickening due to the algebraic decay is clearly evident in Fig. 4.

It is easily verified that shock waves whose upstream and downstream conditions correspond to values of $B<1$ will not have physically realistic structures. This fact was pointed out by Cramer and Kluwick,[5] who also showed that such shocks violate the speed-ordering relation. The latter is also known as the entropy condition.[10] When applied to a

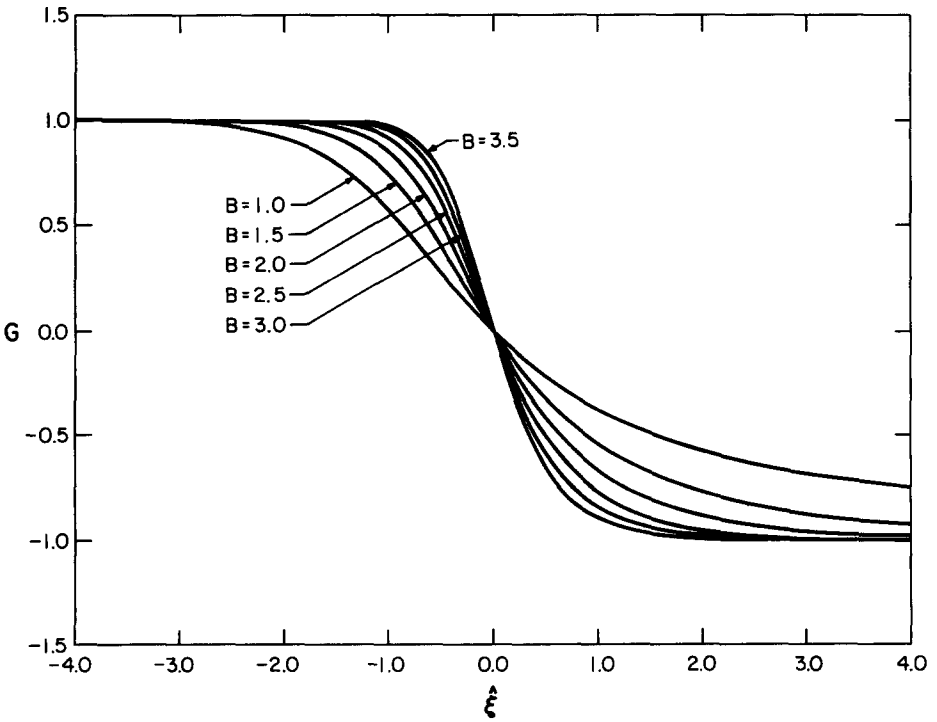

FIG. 4. Plots of function G. Here $B=1$ corresponds to sonic shock.

stationary normal shock this speed-ordering condition requires that the flow be supersonic upstream of the shock and subsonic downstream of the shock; this fact will be verified in Sec. V. When the existence condition $B \geqslant 1$ is violated the proposed discontinuity suffers either a partial or total disintegration.[5,6,8]

In Sec. 5 of Ref. 5 it was pointed out that the entropy inequality will always be satisfied when the dissipative structure exists, i.e., when $B \geqslant 1$. This becomes obvious when the expression for the entropy jump given in Eq. (3.5) of Ref. 5 is combined with the present expression for B; this reads as

$$s_a - s_b \approx (a_0^2 |\Lambda| / 36 T_0) \left[(\rho_a - \rho_b)/\rho_0 \right]^4 B, \qquad (11)$$

where T_0 is the absolute temperature of the unperturbed state.

The shock waves possible when $\bar{\Gamma} \approx 0$ were discussed by Cramer and Kluwick[5] through the use of scaled variables. A more natural and revealing approach is to examine the shock adiabat in the pressure-specific volume $V \equiv 1/\rho$ plane. For the present purposes it will be sufficient to consider only the case where the upstream state is the unperturbed state, i.e., $\rho_b = \rho_0$. To lowest order, the shock adiabat is just a Poisson adiabat, i.e., an isentrope. A completely analogous situation occurs in the analysis of weak shocks in perfect gases. Thus the adiabat may be approximated by

$$\frac{p_a - p_0}{a_0^2 \rho_0} = -\frac{V_a - V_0}{V_0} + \Gamma \left(\frac{V_a - V_0}{V_0} \right)^2 - \frac{\Lambda}{3} \left(\frac{V_a - V_0}{V_0} \right)^3 + O\left[\left(\frac{V_a - V_0}{V_0} \right)^4 \right],$$

where (3) and (11) have been employed and where $\bar{p}$ is thermodynamic pressure. The adiabats for $\Lambda > 0$ and $\Lambda < 0$ have been sketched in Figs. 5 and 6, respectively. It is easily verified that the curvature changes sign when the local value of

$$\bar{\Gamma} \approx \frac{a_0}{\rho_0} \left(\Gamma + \Lambda \frac{\rho_a - \rho_0}{\rho_0} \right) \approx \frac{a_0}{\rho_0} \left(\Gamma - \Lambda \frac{V_a - V_0}{V_0} \right) \qquad (12)$$

changes sign. The shocks which satisfy the existence condition $B \geqslant 1$ are determined by examining the slope of the adiabat at the downstream state,

$$m_a \equiv \frac{dp_a}{dV_a} = -a_0^2 \rho_0^2 \left\{ 1 + \frac{\Lambda B}{3\sigma} \left(\frac{V_a - V_0}{V_0} \right)^2 + O\left[\left(\frac{V_s - V_0}{V_0} \right)^3 \right] \right\}; \qquad (13)$$

the slope of the adiabat at the upstream state,

$$m_b \equiv -a_0^2 \rho_0^2; \qquad (14)$$

and the slope of the chord connecting the upstream and downstream states,

$$m_c \equiv \frac{p_a - p_0}{V_a - V_0} = -a_0^2 \rho_0^2 \left\{ 1 + \frac{\Lambda}{6} \left(\frac{V_a - V_0}{V_0} \right)^2 \times \left(\frac{B}{\sigma} - 1 \right) + O\left[\left(\frac{V_a - V_0}{V_0} \right)^3 \right] \right\}, \qquad (15)$$

where (8) has been used to obtain the final forms of (13) and (15). Inspection of (13)–(15) immediately shows that

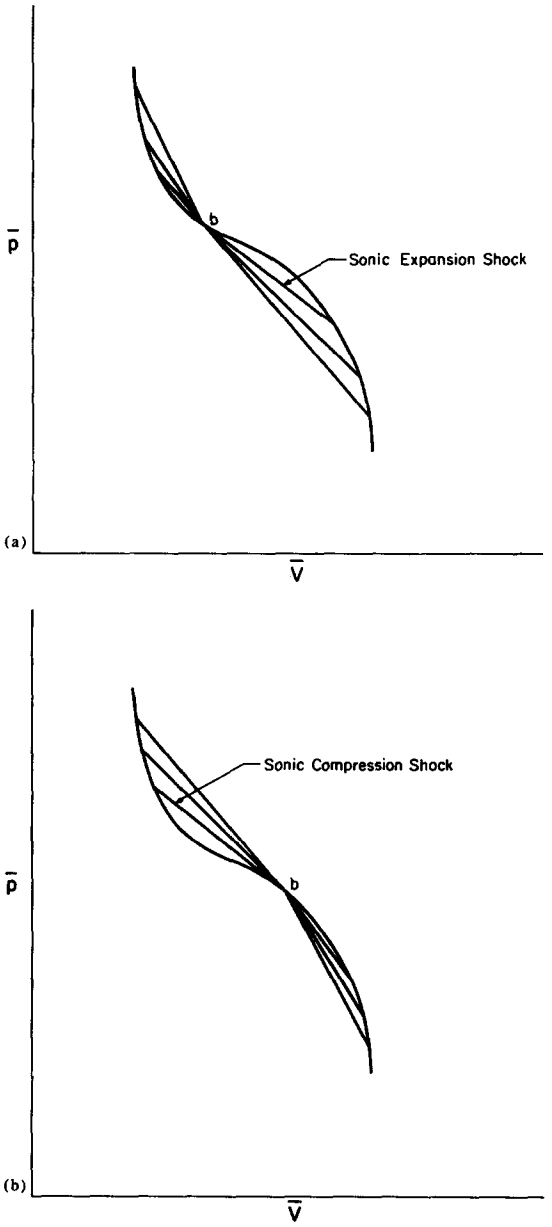

FIG. 5. Shock adiabats for $\Lambda > 0$ and $\rho_b = \rho_0$. The upstream state is denoted by the symbol b. The straight lines connect acceptable upstream and downstream states, i.e., those satisfying (16). (a) $\bar{\Gamma}(\rho_0, s_0) > 0$. (b) $\bar{\Gamma}(\rho_0, s_0) < 0$.

shocks which satisfy $B \geqslant 1$ must also satisfy to the slope-ordering conditions

$$m_b \geqslant m_c > m_a \quad \text{when} \quad \Lambda > 0 \qquad (16)$$

and

$$m_b > m_c \geqslant m_a \quad \text{when} \quad \Lambda < 0. \qquad (17)$$

The equalities correspond to sonic conditions, i.e., $B = 1$. Acceptable shocks, i.e., those satisfying (16) and (17), are depicted in Figs. 5 and 6. For a given upstream state corresponding to $\Lambda > 0$ both expansion and compression shocks are possible. Within the limitations of the weak shock theory, compression shocks of arbitrary magnitude are possible when $\Gamma > 0$, $\Lambda > 0$. Because $\Gamma > 0$, expansion shocks which are relatively weak will result in $m_b < m_c$, in violation of (16). Sufficiently weak expansion shocks may also violate

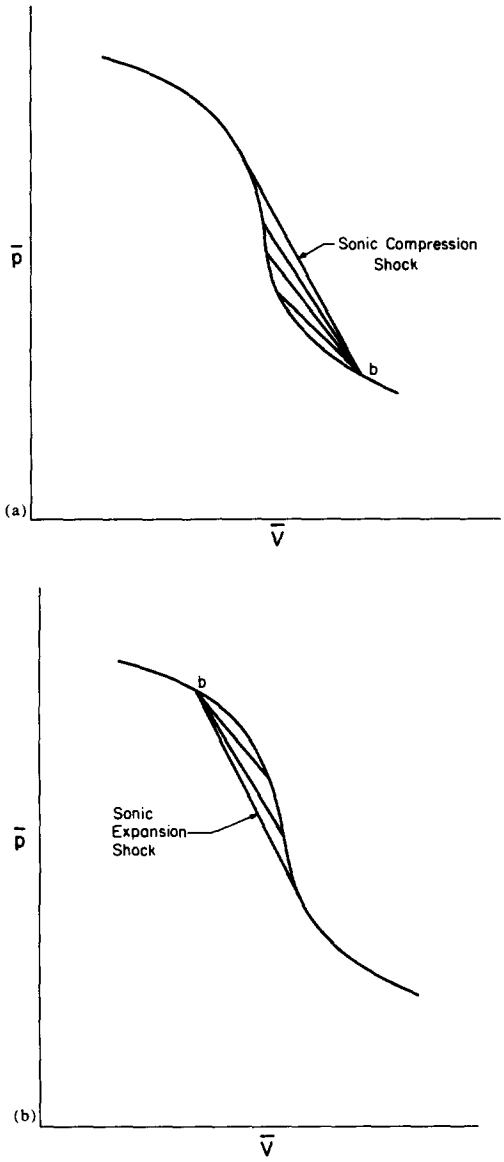

FIG. 6. Shock adiabats for $\Lambda < 0$ and $\rho_b = \rho_0$. The upstream state is denoted by the symbol b. The straight lines connect acceptable upstream and downstream states, i.e., those satisfying (17). (a) $\bar{\Gamma}(\rho_0, s_0) > 0$. (b) $\bar{\Gamma}(\rho_0, s_0) < 0$.

the second inequality in (16), as well as the entropy inequality. Thus there is a lower bound on the strength of expansion shocks when $\Gamma > 0$ and $\Lambda > 0$. This lower bound corresponds to a sonic shock having $B = 1$ and $m_b = m_c > m_a$; the strength of this sonic shock is given by

$$(\rho_a - \rho_0)/\rho_0 = -3\Gamma/\Lambda.$$

Similar observations may be made for the case $\Gamma < 0$, $\Lambda > 0$. When $\Lambda < 0$ only one type of shock is possible for a given upstream state. In this case the limiting shock is also a sonic shock with sonic conditions at the downstream state, i.e., $m_b > m_c = m_a$. Within the context of the present theory this upper bound on the magnitude of the shock strength given by

$$(\rho_a - \rho_0)/\rho_0 = -3\Gamma/2\Lambda.$$

Such slope-ordering conditions have been employed in the present context by Thompson and Lambrakis[4] and Cramer and Sen.[8] Discussions in the context of fluids having $\bar{\Gamma} > 0$ have been given by Landau and Lifshitz.[11]

To relate the details of the structure given by (5)–(10) to the shock waves depicted in Figs. 5 and 6 it is necessary to examine the complicated dependence of B on the shock strength. This is found by solving (8) for the shock strength:

$$\frac{\rho_a - \rho_b}{\rho_0} = \frac{6\sigma}{B - 3\sigma}\left(\frac{\Gamma}{\Lambda} + \frac{\rho_b - \rho_0}{\rho_0}\right). \tag{18}$$

The simplest relation occurs when $\Lambda < 0$, where B varies monotonically from 1 at the sonic condition to infinity in the limit of zero strength. When $\Lambda > 0$ the two types of shocks possible corresponds to the ranges $3 \leqslant B < \infty$ and $1 \leqslant B < 3$. The first range corresponds to the compression shocks illustrated in Fig. 5(a) and the expansion shocks in Fig. 5(b). In each case the strength vanishes as $B \to \infty$ and becomes infinitely large, in either the positive or negative sense, as $B \to 3$. The expansion shocks in Fig. 5(a) and the compression shocks in Fig. 5(b) approach the sonic condition as $B \to 1$ and become infinitely strong in the limit $B \to 3$.

III. SHOCK THICKNESS

The thickness of the shock will be measured by the well-known maximum slope criterion. In terms of the scaled variables this is $-2/G'|_m$, where $G'|_m < 0$ is the minimum value of the slope of the $G = G(\hat{\xi})$ curve. Results (9) and (10) may be employed to show that the dimensional thickness τ is given by

$$\frac{\tau}{L_d} = -\frac{2\Gamma^2}{\Lambda^2}\left(\frac{\rho_0}{\rho_a - \rho_b}\right)^2 \frac{1}{G'|_m}. \tag{19}$$

The results of Sec. 5 of Cramer and Kluwick[5] may be used to show that

$$G'|_m = (G^{*2} - 1)(G^* + B), \tag{20}$$

where

$$G^* = -\tfrac{1}{3}B + (\tfrac{1}{9}B^2 + \tfrac{1}{3})^{1/2}. \tag{21}$$

For a given unperturbed state (8) may be combined with (19)–(21) to determine the variation of τ with the shock strength. In Fig. 7 the variation of the nondimensional thickness $\tau/2L_d$ versus the nondimensional shock strength

$$(\Lambda/\Gamma)[(\rho_a - \rho_b)/\rho_0]$$

has been plotted for the special case where the upstream state is also the unperturbed state, i.e., $\rho_b = \rho_0$.

The most striking and important feature of Fig. 7 is the nonmonotonic variation of the thickness when $\Lambda < 0$. The local minimum in the thickness occurs in both the compression and expansion shocks depicted in Fig. 6. Straightforward differentiation of (19) shows that this minimum occurs at

$$(\rho_a - \rho_0)/\rho_0 = -(\tfrac{9}{8})^{1/2}\Gamma/\Lambda.$$

A comparison with (12) reveals that the minimum thickness occurs just after the local value of $\bar{\Gamma}$ changes sign across the shock. The physical reason for this phenomenon is that the tendency to thicken as the sonic condition is approached balances and then overwhelms the usual tendency of the shock to become thinner with increasing strength. This

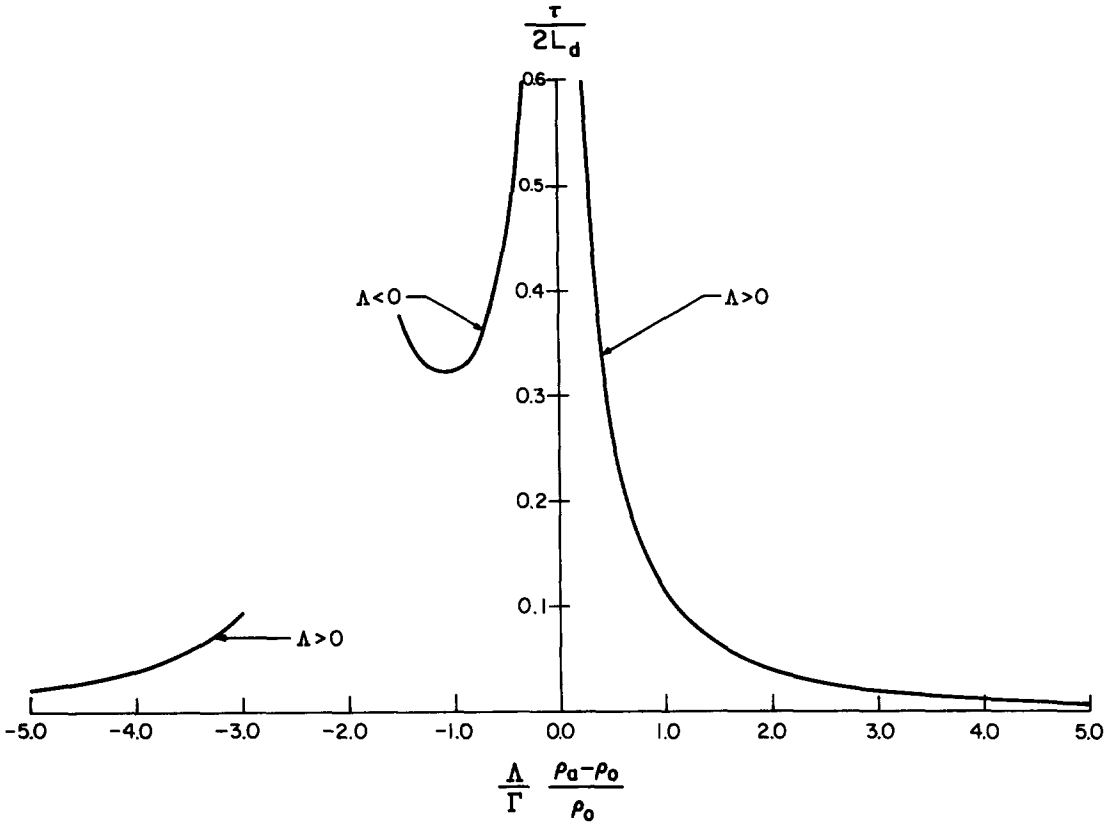

FIG. 7. Plot of scaled shock thickness versus scaled strength.

thickening also occurs when $\Lambda > 0$. However, it is not apparent in Fig. 7 because the sonic condition can only be approached by reducing the strength of the shock; both effects tend to thicken the shock. The branch of the $\Lambda > 0$ curve corresponding to positive values of $\Lambda(\rho_a - \rho_0)/\Gamma\rho_0$ does not contain a sonic shock and appears similar to the classical variation.

As an example, we consider the case where $\Lambda < 0$. The thickness of the sonic shock is $\tau = 0.75L_d$, whereas a shock of one-half its strength, i.e.,

$$(\rho_a - \rho_0)/\rho_0 = 3\Gamma/4|\Lambda|,$$

is actually thinner, with a width equal to $\tau \approx 0.70L_d$.

The thickening effect described here should be distinguished from that caused by variations in the viscosity with temperature. The shock is taken to be weak and the dissipation coefficients have been approximated by the values at the unperturbed state. In finite amplitude shocks, both effects will need to be considered.

IV. ENTROPY DISTRIBUTION

To lowest order, the variation of entropy in any weak shock may be approximated by

$$\bar{s} - s_b \approx -\frac{1}{\mathrm{Pr}} \frac{\mu_0 \beta_0 a_0}{\rho_0^2} \frac{d\bar{\rho}}{d\bar{x}}, \tag{22}$$

where β_0 is the coefficient of thermal expansion

$$\bar{\beta} = -\frac{1}{\bar{\rho}} \frac{\partial \bar{\rho}}{\partial \bar{T}}\bigg|_{\bar{p}}$$

evaluated at the unperturbed state; in all that follows β_0 is taken to be positive. Equation (22) is valid for small values of $\bar{\Gamma}$, as well as values of order 1; an equivalent result is given in Sec. 87 of Landau and Lifshitz.[11] To the accuracy of (22) $\bar{s} \to s_b$ as $\bar{x} \to \pm\infty$. This is because of the well-known fact that the entropy variation inside a shock layer is always an order of magnitude larger than the ultimate rise across the shock. Results obtained through the use of (22) will therefore be the correct lowest-order variation within the shock layer. The overall entropy rise across the shock must be obtained by reference to more accurate expressions such as (11); this was obtained by an examination of the higher-order terms neglected in (22).

In the coordinate system used here the upstream conditions are attained as $\bar{x} \to \infty$. Thus compression shocks will have $d\bar{\rho}/d\bar{x} < 0$ and $\bar{s} > s_b$ at every $\bar{x}$. To the accuracy implicit in (22), expansion shocks result in an entropy deficit throughout the shock, i.e., $\bar{s} < s_b$ at every finite $\bar{x}$. Acceptable shocks will result in a net increase in entropy across the shock and the entropy distribution of weak expansion and compression shocks will appear as shown in Fig. 8.

Detailed solutions for the entropy variation are obtained by substituting the density distribution in (22). In the present case, (5), (6), (9), and (10) are combined with (22); the entropy is then found to be

$$\bar{s} - s_b = -\frac{\beta_0 a_0^2 |\Lambda|}{24\,\mathrm{Pr}[\lambda_0/\mu_0 + 2 + (\gamma_0 - 1)/\mathrm{Pr}]} \times [(\rho_a - \rho_b)/\rho_0]^3 G'(\hat{\xi}). \tag{23}$$

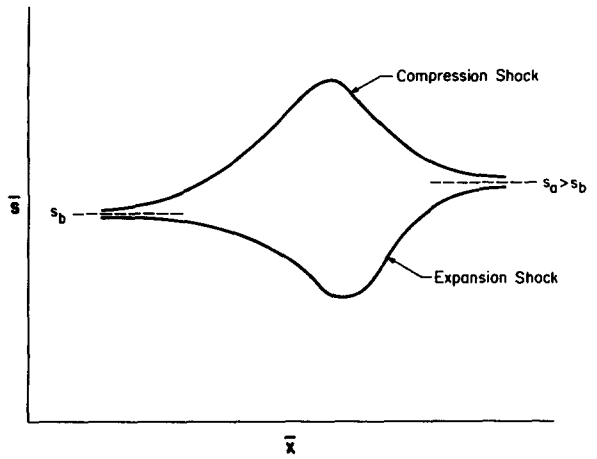

FIG. 8. Comparison of entropy distribution through expansion and compression shocks. In this sketch, upstream conditions are at left ($\bar{x} \to -\infty$) and downstream conditions are at right ($\bar{x} \to \infty$).

Because $G' < 0$, (23) gives a direct relation between the sign of $\bar{s} - s_b$ and the density jump. A result more convenient for plotting may be obtained by straightforward differentiation of (6) and use of (18); this reads as

$$\bar{s} - s_b = \frac{9\beta_0 \mu_0^2 \Gamma^3}{\mathrm{Pr}[\lambda_0/\mu_0 + 2 + (\gamma_0 - 1)/\mathrm{Pr}]\Lambda^2} \times \left(1 + \frac{\Lambda}{\Gamma}\frac{\rho_b - \rho_0}{\rho_0}\right)^3 \frac{(1 - G^2)(G + B)}{(B - 3\sigma)^3}. \quad (24)$$

When the upstream state is the undisturbed state, i.e., $\rho_b = \rho_0$, an appropriate scaled version of the entropy is

$$\hat{s} \equiv (\Gamma/|\Gamma|)[(1 - G^2)(G + B)/(B - 3\sigma)^3], \quad (25)$$

where $\Gamma/|\Gamma|$ is introduced to account for the sign of Γ. This scaled entropy is plotted in Fig. 9 for the case where $\Gamma > 0$, $\Lambda > 0$. The horizontal scale is taken to be $\hat{\xi}\sigma$. Thus the upstream state is always approached as $\sigma\hat{\xi} \to \infty$ and the downstream state is approached as $\sigma\hat{\xi} \to -\infty$. The curves in which $3 \leqslant B < \infty$ correspond to the compression shocks in Fig. 5(a) and those in which $1 \leqslant B < 3$ correspond to the expansion shocks. The entropy variations of the shocks shown in Fig. 6(a) are plotted in Fig. 10.

In the interpretation of Figs. 9 and 10, it is useful to note that $\hat{\xi}$ has been scaled with the shock strength; see, e.g., (9). Thus the thickening as the shock weakens, i.e., as $B \to \infty$, has been masked in these plots.

The general behavior depicted in Fig. 8 is also expected to be typical of finite amplitude expansion shocks. Near the upstream and downstream asymptotes, the energy equation may be approximated by

$$mT_i \frac{d\bar{s}}{d\bar{x}} \approx k_i \frac{d^2\bar{T}}{d\bar{x}^2}, \quad (26)$$

where $m > 0$ is the constant mass flux and $\bar{k} > 0$ denotes the thermal conductivity. Here we have recognized that the viscous dissipation is necessarily of higher order as the asymptotes are approached. If the approximation is made near the downstream asymptote $(T_i, k_i) = (T_a, k_a)$, and if it is made near the upstream asymptote $(T_i, k_i) = (T_b, k_b)$. If the absolute temperature $\bar{T}$ is assumed to decrease monotonically through expansion shocks and the flow direction is in the positive $\bar{x}$ direction, (26) implies $d\bar{s}/d\bar{x} < 0$ near the upstream asymptote ($\bar{x} \to -\infty$) and $d\bar{s}/d\bar{x} > 0$ near the downstream asymptote ($\bar{x} \to \infty$). If only one extremum of $\bar{s}$ is expected, the entropy distribution is as indicated in Fig. 8. It is easily verified that these arguments are consistent with the well-known distribution for finite amplitude compression shocks.

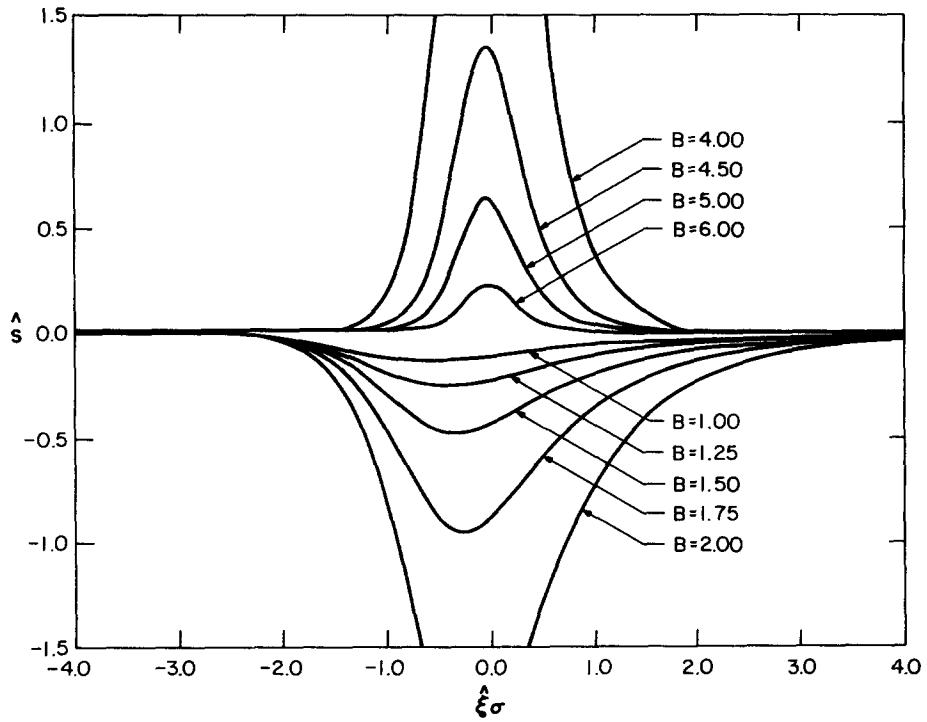

FIG. 9. Plots of scaled entropy for $\Lambda > 0$, $\Gamma > 0$, and $\rho_b = \rho_0$. Shocks correspond to those found in Fig. 5(a). Upstream conditions are at right.

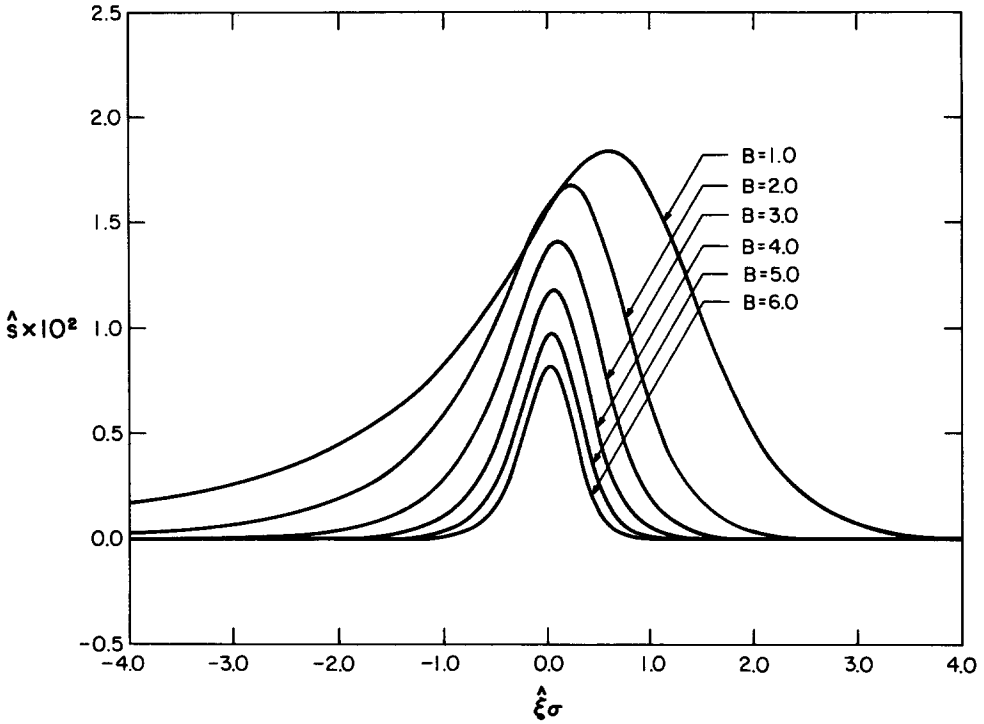

FIG. 10. Plots of scaled entropy for $\Lambda<0$, $\Gamma>0$, and $\rho_b=\rho_0$. Shocks correspond to those found in Fig. 6(a). Upstream conditions are at right.

V. MACH NUMBER DISTRIBUTION

The analysis of Cramer and Kluwick[5] was carried out in a coordinate system moving with the shock speed $\bar{u}$. In such a coordinate system the appropriate definition of the local Mach number is

$$M\equiv(\bar{u}-\bar{v})/\bar{a}, \tag{27}$$

where $\bar{v}$ is the particle velocity relative to the rest frame. The shock speed is obtained directly from the inviscid computations[5]; this is seen to be

$$\frac{\bar{u}}{a_0}=1+\frac{\Gamma}{2}\left(\frac{\rho_a-\rho_0}{\rho_0}+\frac{\rho_b-\rho_0}{\rho_0}\right)+\frac{\Lambda}{6}\left[\left(\frac{\rho_a-\rho_0}{\rho_0}\right)^2+\left(\frac{\rho_a-\rho_0}{\rho_0}\right)\left(\frac{\rho_b-\rho_0}{\rho_0}\right)+\left(\frac{\rho_b-\rho_0}{\rho_0}\right)^2\right]+O\left[\left(\frac{\bar{\rho}-\rho_0}{\rho_0}\right)^3\right]. \tag{28}$$

The expressions for the particle velocity and sound speed in the shock layer were found to be

$$\frac{\bar{v}}{a_0}=\frac{\bar{\rho}-\rho_0}{\rho_0}-\left(\frac{\bar{\rho}-\rho_0}{\rho_0}\right)^2+O\left[\left(\frac{\bar{\rho}-\rho_0}{\rho_0}\right)^3\right], \tag{29}$$

$$\frac{\bar{a}}{a_0}=1+(\Gamma-1)\frac{\bar{\rho}-\rho_0}{\rho_0}+\left(1+\frac{\Lambda}{2}\right)\left(\frac{\bar{\rho}-\rho_0}{\rho_0}\right)^2+O\left[\left(\frac{\bar{\rho}-\rho_0}{\rho_0}\right)^3\right]. \tag{30}$$

Although these results were not given explicitly in Sec. 5 of Ref. 5, Eq. (30) can be recognized as a straightforward Taylor series expansion of $\bar{a}/a_0$. Here it is necessary to note that the entropy deviation is of third order in the density perturbation inside the shock layer although the overall entropy rise (11) is of fourth order. The corresponding quantities in perfect gas theory are second and third order, respectively. When (28)–(30) are substituted in (27) the local Mach number in the shock layer may be approximated by

$$M=1-\frac{\Lambda}{8}\left(\frac{\rho_a-\rho_b}{\rho_0}\right)^2\left(G^2+\frac{2}{3}GB-\frac{1}{3}\right)+O\left[\left(\frac{\rho_a-\rho_b}{\rho_0}\right)^3\right], \tag{31}$$

where (5) and (8) have been used. Equation (5) may also be employed to show that the upstream conditions are obtained as $G\to-1/\sigma$. In this limit (31) reduces to the following expression for the upstream Mach number:

$$M_b=1-(\Lambda/12)[(\rho_a-\rho_b)/\rho_0]^2(1-B/\sigma). \tag{32}$$

The downstream Mach number is obtained in the limit $G\to1/\sigma$:

$$M_a=1-(\Lambda/12)[(\rho_a-\rho_b)/\rho_0]^2(1+B/\sigma). \tag{33}$$

When the unperturbed state is such that $\Lambda>0, \sigma=1$ the existence condition $B\geqslant1$ may be combined with (32) and (33) to show that

$$M_b\geqslant1>M_a.$$

In a like manner,

$$M_b>1\geqslant M_a$$

when $\Lambda<0$. This verifies the claim, made in Sec. II, that the condition for the existence of the structure ($B\geqslant1$) requires a supersonic–subsonic transition across the shock.

The upstream and downstream Mach numbers may also be related to the relative slopes of the shock adiabat. When the slopes (13)–(15) are recast in terms of the density perturbations and combined with (32) and (33) we find

$$M_b - 1 = (m_b - m_c)/2a_0^2\rho_0^2,$$

$$M_a - 1 = (m_a - m_c)/2a_0^2\rho_0^2$$

to lowest order.

The following scaled version of the Mach number may be formed by combining (31)–(33):

$$\frac{M - M_a}{M_b - M_a} = -\frac{3\sigma}{4B}\left(G^2 + \frac{2}{3}GB - 1 - \frac{2B}{3\sigma}\right). \quad (34)$$

This has been plotted in Fig. 11 for the case $\Lambda > 0$ and in Fig. 12 for $\Lambda < 0$. The scaled Mach number (34) will always approach 1 at the upstream state and zero at the downstream state. In the theory of perfect gases, the Mach number varies monotonically between its upstream and downstream values. The new feature portrayed here is that the Mach number may attain a local maximum or minimum inside the shock. The slope of the Mach number curve may be obtained directly from (31); this is found to be

$$\frac{dM}{d\hat{\xi}} = -\frac{G'\sigma}{2}\frac{\rho_a - \rho_b}{\rho_0}\left(\Gamma + \Lambda\frac{\bar{\rho} - \rho_0}{\rho_0}\right). \quad (35)$$

A comparison of (35) with (12) shows that M must attain an extremum whenever the local value of the fundamental derivative (1) changes sign. Thus the Mach number of each expansion shock in Fig. 5(a) and each compression shock in Fig. 5(b) will have a local maximum where $\bar{\Gamma}$ changes sign inside the shock. The Mach number variations for $B = 1$–3 in Fig. 11 are typical of these shocks. The remaining profiles $3 \leqslant B < \infty$ correspond to the compression shocks in Fig. 5(a) and the expansion shocks in Fig. 5(b). The sign of $\bar{\Gamma}$ does not change across these shocks and the variation is monotonic. When $\Lambda < 0$ shocks having $\infty > B \geqslant 3$ are relatively weak and do not result in a change in sign of $\bar{\Gamma}$ across the shock. Inspection of Fig. 12 shows the expected result that the Mach number variation is monotonic. Stronger shocks ($1 \leqslant B \leqslant 3$) result in a change in sign of $\bar{\Gamma}$ and the Mach number attains the local minimum depicted in Fig. 12.

As in the plots of the entropy distribution, the thickening of the shock as the strength vanishes is not apparent in Figs. 11 and 12; this is due to the scaling (9).

VI. SUMMARY

The present study has extended the previous investigations[4,5] of the dissipative structure of shock waves propagating in fluids of large specific heat. As in the previous studies, the results of interest have been obtained for fairly general gas models. The main assumption concerning the equation of state is that an embedded region of negative nonlinearity, similar to that depicted in Fig. 1, exists. Two nonclassical features of shocks across which the fundamental derivative changes sign have been described. A class of compression and expansion shocks have been found in which the thickness is no longer a monotone decreasing function of strength. This is due to the slow approach to the inviscid conditions associated with sonic and near-sonic shocks. It was also shown that the local Mach number attains either a maximum or minimum when the local value of the fundamental derivative changes sign across the shock; this contrasts with the monotone variation known to occur in perfect gases.

In Sec. IV the entropy distribution within the shock layer has been derived. The variation in expansion shocks is seen to be nonclassical in the sense that the local value of the entropy is less than the upstream value over most of the shock layer. This entropy difference $\bar{s}(\bar{x}) - s_b$ ultimately changes sign and approaches the positive downstream value given by (11). This result is not directly related to the change in sign of $\bar{\Gamma}$; rather, it occurs for any expansion shock.

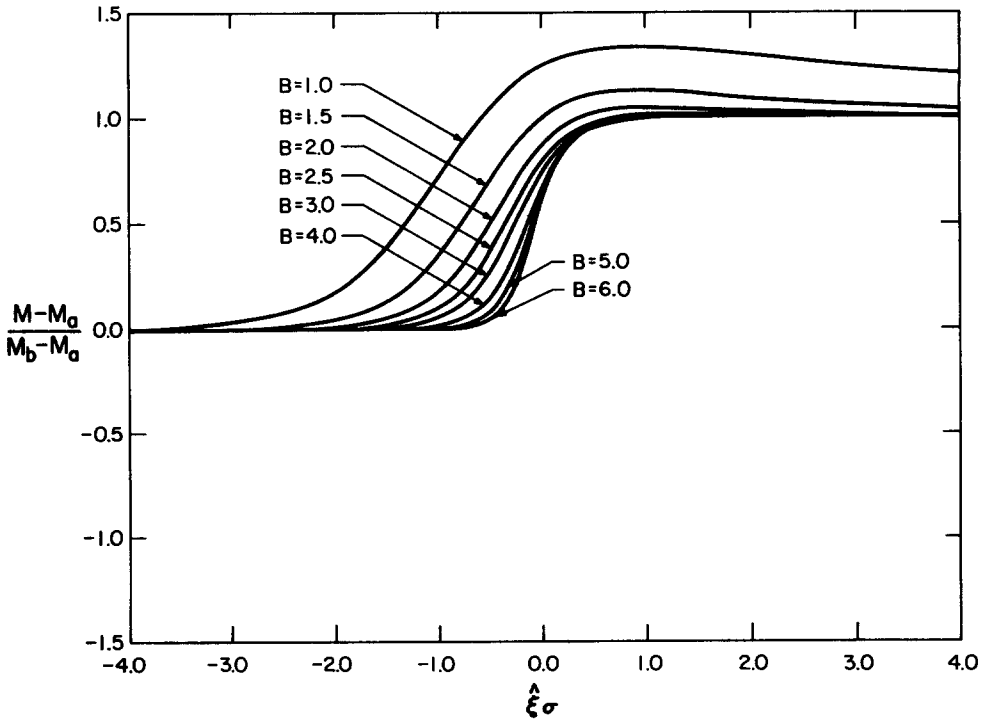

FIG. 11. Plots of scaled Mach numbers for $\Lambda > 0$ and $\rho_b = \rho_0$. Upstream conditions are at right.

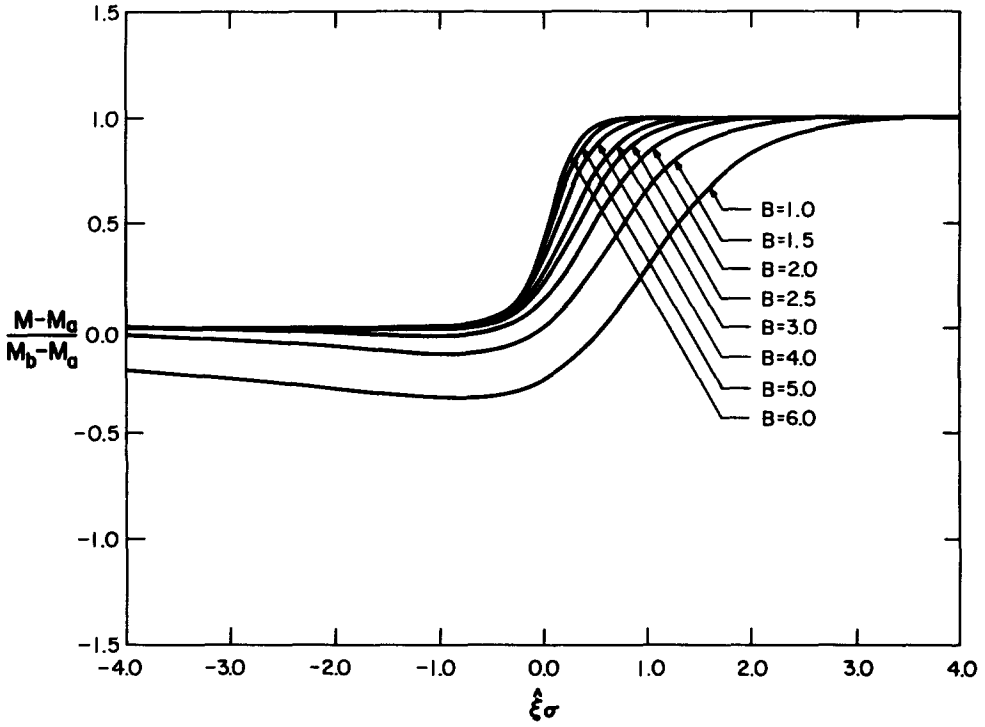

FIG. 12. Plots of scaled Mach numbers for $\Lambda<0$ and $\rho_b=\rho_0$. Upstream conditions at right.

Although the shocks described here are restricted to relatively small amplitude, many of the qualitative features are expected to appear in shocks of larger strength. Arguments which extend the results for the entropy to finite amplitude shocks are given in Sec. IV. Furthermore, analogous behavior can also be expected in materials other than the single-phase gases treated here, e.g., the viscoelastic solids described by Lee-Bapty[9] and the temperature shock in superfluid helium.[12]

ACKNOWLEDGMENT

The author would like to thank R. Sen for the calculations and plotting leading to Figs. 1–3.

APPENDIX: EXPLICIT EXPRESSIONS FOR Λ

In terms of the specific volume $\overline{V}\equiv\bar{\rho}^{-1}$ and absolute temperature $\overline{T}$, the fundamental derivative (1) may be written[1,3,4]

$$\overline{\Gamma}=\frac{\overline{V}^4}{2\bar{a}}\left[\bar{P}_{\overline{V}\overline{V}}-\frac{3\overline{T}}{\bar{c}_v}\bar{p}_{\overline{T}}\bar{p}_{\overline{V}\overline{T}}+\frac{3\overline{T}^2}{\bar{c}_v^2}(\bar{p}_{\overline{T}})^2\bar{p}_{\overline{T}\overline{T}}+\frac{\overline{T}}{\bar{c}_v^2}(\bar{p}_{\overline{T}})^3\left(1-\frac{\overline{T}}{\bar{c}_v}\frac{\partial\bar{c}_v}{\partial\overline{T}}\right)\right],$$

where $\bar{c}_v=\bar{c}_v(\overline{V},\overline{T})$ is the specific heat at constant volume and $\bar{a}=\bar{a}(\overline{V},\overline{T})$ is the thermodynamic sound speed given by

$$\bar{a}=\overline{V}\left[(\overline{T}/\bar{c}_v)(\bar{p}_{\overline{T}})^2-\bar{p}_{\overline{V}}\right]^{1/2}.$$

The subscripts $\overline{T}$ and $\overline{V}$ on the pressure $\bar{p}(\overline{V},\overline{T})$ denote partial derivatives with respect to $\overline{V}$ and $\overline{T}$. The quantity $\partial\bar{c}_v/\partial\overline{T}$ is the derivative of $\bar{c}_v$ with $\overline{V}$ held constant. In a like manner, the derivative (2) may be shown to be

$$\Lambda=-\frac{\overline{\Gamma}}{\bar{a}\overline{V}}\left(3+\frac{\overline{\Gamma}}{\overline{V}\bar{a}}\right)+\frac{\overline{V}^4}{2\bar{a}^2}\left(D_V-\frac{\overline{T}}{\bar{c}_v}\bar{p}_{\overline{T}}D_T\right),$$

where

$$D_V\equiv-\frac{\partial}{\partial\overline{V}}\left(\frac{2\,\overline{a}\overline{\Gamma}}{\overline{V}^4}\right)$$

$$=-\bar{p}_{\overline{V}\overline{V}\overline{V}}+\frac{3\overline{T}}{\bar{c}_v}(\bar{p}_{\overline{T}}\bar{p}_{\overline{V}\overline{T}})_{\overline{V}}+\frac{\overline{T}^2}{\bar{c}_v^2}\left[\frac{3(\bar{p}_{\overline{T}})^2\bar{p}_{\overline{T}\overline{V}}}{\overline{T}}\left(\frac{\overline{T}}{\bar{c}_v}\frac{\partial\bar{c}_v}{\partial\overline{T}}-1\right)-3\left[(\bar{p}_{\overline{T}})^2\bar{p}_{\overline{T}\overline{T}}\right]_{\overline{V}}-3\bar{p}_{\overline{T}}\bar{p}_{\overline{T}\overline{T}}\bar{p}_{\overline{T}\overline{V}}\right]$$

$$+\frac{\overline{T}^3}{\bar{c}_v^3}\left[\frac{(\bar{p}_{\overline{T}})^3\left(\overline{T}\bar{p}_{\overline{T}\overline{T}}\right)_{\overline{T}}}{\overline{T}}+6(\bar{p}_{\overline{T}\overline{T}}\bar{p}_{\overline{T}})^2+\frac{(\bar{p}_{\overline{T}})^3\bar{p}_{\overline{T}\overline{T}}}{\overline{T}}\left(2-3\frac{\overline{T}}{\bar{c}_v}\frac{\partial\bar{c}_v}{\partial\overline{T}}\right)\right]$$

and

$$D_T\equiv-\frac{\partial}{\partial\overline{T}}\left(\frac{2\,\overline{a}\overline{\Gamma}}{\overline{V}^4}\right)=-\bar{p}_{\overline{V}\overline{V}\overline{T}}+\frac{3\overline{T}}{\bar{c}_v}\left[(\bar{p}_{\overline{T}}\bar{p}_{\overline{V}\overline{T}})_{\overline{T}}+\frac{\bar{p}_{\overline{T}}\bar{p}_{\overline{V}\overline{T}}}{\overline{T}}\left(1-\frac{\overline{T}}{\bar{c}_v}\frac{\partial\bar{c}_v}{\partial\overline{T}}\right)\right]$$

$$+\frac{\overline{T}^2}{\overline{c}_v^2}\left[\frac{(\overline{p}_{\overline{T}})^3}{\overline{T}^2}\left(1-\frac{\overline{T}}{\overline{c}_v}\frac{\partial\overline{c}_v}{\partial\overline{T}}\right)\left(\frac{3\overline{T}}{\overline{c}_v}\frac{\partial\overline{c}_v}{\partial\overline{T}}-1\right)-\frac{9(\overline{p}_{\overline{T}})^2\overline{p}_{\overline{T}\overline{T}}}{\overline{T}}\left(1-\frac{\overline{T}}{\overline{c}_v}\frac{\partial\overline{c}_v}{\partial\overline{T}}\right)\right.$$
$$\left.-3\left[(\overline{p}_{\overline{T}})^2\overline{p}_{\overline{T}\overline{T}}\right]_{\overline{T}}\right]+\frac{\overline{T}^2(\overline{p}_{\overline{T}})^3}{\overline{c}_v^3}\frac{\partial^2\overline{c}_v}{\partial\overline{T}^2}.$$

In order to obtain the variation of $\overline{\Gamma}$ and Λ with respect to density at constant entropy, the equation of state should be used to evaluate the temperature $\overline{T}=\overline{T}(\overline{V},\overline{s})$ at constant $\overline{s}$. This, along with $\overline{V}$, is then substituted in the above expressions for $\overline{a}$, $\overline{\Gamma}$, and Λ.

[1]See National Technical Information Service Document No. PB 032189 (Office of Scientific Research and Development Rep. No. 545). Copies are available at the U.S. Library of Congress, Washington, D.C. 20540, under the NTIS number.

[2]Y. B. Zel'dovich, Zh. Eksp. Teor. Fiz. **4**, 363 (1946).

[3]K. C. Lambrakis and P. A. Thompson, Phys. Fluids **5**, 933 (1972).

[4]P. A. Thompson and K. C. Lambrakis, J. Fluid Mech. **60**, 187 (1973).

[5]M. S. Cramer and A. Kluwick, J. Fluid Mech. **142**, 9 (1984).

[6]M. S. Cramer, A. Kluwick, L. T. Watson, and W. Pelz, J. Fluid Mech. **169**, 323 (1986).

[7]M. S. Cramer and R. Sen, Phys. Fluids **29**, 2181 (1986).

[8]M. S. Cramer and R. Sen, Phys. Fluids **30**, 377 (1987).

[9]I. P. Lee-Bapty, Ph.D. thesis, Leeds University, 1981.

[10]P. D. Lax, *Contributions to Nonlinear Functional Analysis* (Academic, New York, 1971).

[11]L. D. Landau and E. M. Lifshitz, *Fluid Mechanics* (Addison–Wesley, Reading, MA, 1959).

[12]T. N. Turner, Ph.D. thesis, California Institute of Technology, 1979.